



Numerical modeling of indoor environment with a ceiling fan and an upper-room ultraviolet germicidal irradiation system



Shengwei Zhu ^{a,*}, Jelena Srebric ^b, Stephen N. Rudnick ^c, Richard L. Vincent ^d, Edward A. Nardell ^{c,e}

^a School of Architecture and Urban Planning, Huazhong University of Science and Technology, 1037 Luoyu Road, Hongshan District, Wuhan, Hubei 430074, PR China

^b Department of Architectural Engineering, The Pennsylvania State University, State College, PA, USA

^c Department of Environmental Health, Harvard School of Public Health, Boston, MA, USA

^d Mount Sinai School of Medicine, New York, NY, USA

^e Brigham and Women's Hospital, Boston, MA, USA

ARTICLE INFO

Article history:

Received 13 July 2013

Received in revised form

21 October 2013

Accepted 30 October 2013

Keywords:

Upper-room ultraviolet germicidal irradiation

Ceiling fan

Computational fluid dynamics

Airborne infection control

Fraction of microorganism remaining

ABSTRACT

This study proposes a numerical modeling method for the indoor environment with ceiling fans and upper-room ultraviolet germicidal irradiation (UR-UVGI) fixtures. The numerical modeling deployed steady-state Computational Fluid Dynamics (CFD) with a rotating reference frame to simulate the rotation of fan blades. CFD was validated with experimental data of velocity field and fraction of microorganism remaining at the exhaust diffuser. The fraction of microorganism remaining represented the ratio of the concentration of airborne microorganisms measured with UVGI turned on to the one measured with UVGI turned off. According to the validation results, the CFD model correctly reproduced the air movement induced by the rotation of ceiling fan. When the ambient ventilation rate was 2 ACH (air changes per hour) or 6 ACH, the CFD model accurately predicted the average vertical speeds in the section 2.44 m above the floor with the errors less than 10%, regardless of the ceiling fan's rotational direction or speed. In addition, the simulation results showed that the fraction of microorganism remaining increased with the ambient air exchange rate when the fan blew air downward with a rotational speed as high as 235 rpm, which corresponded with the experimental results. Furthermore, the simulation results accurately predicted the fraction of microorganism remaining when the ambient air exchange rate was 2 ACH. We conclude that this novel numerical model can reproduce the effects of ceiling fans and UR-UVGI fixtures on indoor environment, and should aid in the investigation of the impact of ceiling fans on UR-UVGI disinfection efficacy.

© 2013 Elsevier Ltd. All rights reserved.

1. Introduction

Tuberculosis (TB) is the second leading infectious cause of death worldwide. In 2011, there were estimated 8.7 million incident cases resulting in 1.0 million deaths from TB among HIV-negative people and an additional 0.43 million HIV-positive people [1]. In recent years, the prevalence of multidrug resistant (MDR) TB strains and extensively drug resistant (XDR) TB strains [2,3], has prompted a resurgence of interest in using engineering measures to control the spread of TB, which is usually transmitted from person to person via airborne particles. This interest includes the use of ultraviolet germicidal irradiation (UVGI) to inactivate the infectious particles

by damaging the DNA of the microorganisms. Extensive experimental evidence supports the efficacy of upper-room germicidal ultraviolet air disinfection for airborne infection control [4], including tuberculosis under hospital conditions [5].

Wells et al. first demonstrated the effectiveness of upper-room UVGI (UR-UVGI) to reduce measles transmission in schools [6]. In such a system, UV fixtures are suspended from the ceiling or mounted on a wall in order to flood the upper portion of the room above people's heads with a high irradiation levels while controlling the UV irradiation level in the lower occupied portion of the room. Obviously, the performance of such a system relies greatly on vertical air mixing to transfer infectious airborne particles to the upper portion of the room. In the 1970s, Riley et al. conducted several room-size chamber experiments demonstrating the ability of UR-UVGI to reduce the concentration of airborne microorganisms [7–9]. They found that the UR-UVGI's disinfection rate could

* Corresponding author. Tel.: +86 18071748880.

E-mail address: szhu@hust.edu.cn (S. Zhu).

be increased by using a slow speed large-blade ceiling fan to promote air mixing as long as the fan did not oppose the air motion that was taking place through convection. In the early 2000s, First et al. conducted a series of experiments in a model chamber, similar in size to a single patient isolation room, to investigate the fundamental factors that could affect the disinfection outcome of UR-UVGI fixtures [10,11]. A ceiling fan was used to generate different vertical air mixing conditions in the experiments. According to the report, the operation of the fan resulted in improved inactivation of airborne microorganisms, sometimes at very high rates. Most recently, a study conducted in Peru has found that UR-UVGI with ceiling fans can be 70–80% effective in disinfecting air [5]. Therefore, ceiling fans should be considered an essential adjunct in the application of UR-UVGI, especially in the resource-limited countries and areas. Low velocity ceiling fans are commonly used in warm climates for comfort. They are quiet, efficient, relatively inexpensive, and long-lasting. However, the optimal application of ceiling fans to maximize the UR-UVGI air disinfection is not known.

Computation Fluid Dynamics (CFD) is a potentially useful tool with which to investigate the optimal use of ceiling fans for UR-UVGI disinfection efficacy. There have been a large number of studies about CFD modeling of UR-UVGI [12–14]; however, none of these studies included ceiling fans. We found only one report related to CFD modeling of a ceiling fan [15,16]. In that study, the ceiling fan was replaced by two virtual planes—one 20 cm above the ceiling fan and one 20 cm below the ceiling fan, of which the detailed boundary conditions, such as velocity and turbulent parameters, were obtained from physical measurements. While seemingly applicable, this approach is not appropriate for general application because the user must make many measurements for modeling different ceiling fans, and the air movement between the two virtual planes is neglected. Therefore, there is a need to introduce a new CFD modeling method for ceiling fans that can be easily applied to any kind of ceiling fan, and will be available for a parametric investigation of ceiling fan effects on air disinfection with UR-UVGI.

In this study, a steady-state CFD method with a rotating reference frame to model the rotation of the ceiling fan was proposed for parametrical investigation of ceiling fans' impacts on air mixing and UR-UVGI disinfection efficacy. This method can also be used to examine the popular numerical methods to estimate UV dose and evaluate UV disinfection efficacy in an indoor environment with ceiling fans [17]. In this paper, we fully validated the CFD modeling method of the ceiling fan by experimental data in terms of air velocity and the fraction of microorganism remaining.

2. Methods

The simulation model was validated by the comparison with the experimental results from two independent studies: one by Momoi et al. [15], which measured air velocity's spatial distribution induced by a ceiling fan, and another by First et al. [10], which measured average vertical air speed at a specific height and fraction of microorganism remaining at the exhaust diffuser. They defined the fraction of microorganism remaining as the ratio of the steady-state viable microorganism concentration measured with the UVGI turned on, to the concentration measured with UVGI turned off.

2.1. Room model

The room model in CFD simulations is shown with surface meshes in Fig. 1. It was based on an environmental chamber used by First et al. [10,11]. The chamber had 4.6 m by 2.97 m floor area and a 3.05 m high ceiling, which was about the size of a single-person hospital isolation room. The volume of the simulation field was 41.6 m³. The rotational region, which was directly impacted by

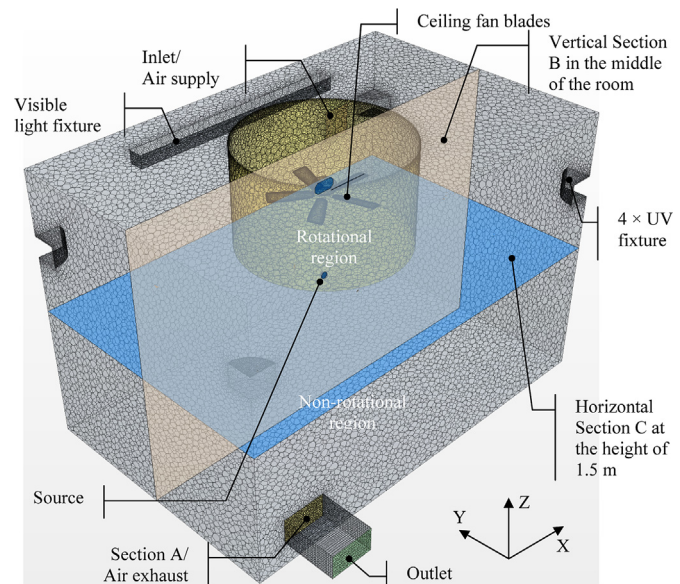


Fig. 1. Room model.

rotation of fan blades, was separated from the non-rotational region by a cylindrical interface that was located in the middle of the room and connected to the ceiling. After a number of trial simulations, the interface was sized with 1.8 m in diameter and 1.1 m in height. As a result, the rotational region occupied around 6.7% of the simulation field.

The room was ventilated by a system that supplied clean air near the ceiling and exhausted contaminated air close to the floor. Clean air was supplied to the room by a ventilation grill that was divided into two nearly equal louvered areas: 55% of the area had louvers directing the exiting air parallel to the adjacent wall, and 45% of the grill area had louvers directing exiting air away from the adjacent wall at 30° angle. As shown in Fig. 1, the outlet of the room model was extended 0.6 m from the exhaust grill, in order to avoid the intervention by the reversed flow from the outlet to indoors. A ceiling fan, capable of rotating at speeds of 80 rpm, 150 rpm, or 235 rpm and blowing air upward or downward, was mounted at the center of the ceiling with the bottom of the motor at a height of 2.5 m above the floor. At each corner there was one 36-W UVGI fixture with its bottom mounted 2.12 m above the floor. In the simulations, it was assumed that the UV irradiation was confined to an upper-room zone 1.8 m–2.6 m above the floor. In addition, a 190-W visible light fixture was mounted on the ceiling. The source of airborne microorganisms was represented in the simulation by a ball with a diameter of 0.146 m at a height of 1.5 m above the floor, located at the center of the room.

2.2. Simulation cases

The six cases that were simulated are listed in Table 1. Cases 1 and 2 were used to validate the model in terms of fan-induced

Table 1
Simulation cases.

Case	Air exchange rate [ACH]	Fan rational direction	Fan rotational speed [rpm]
1	0.5	Upward	160 rpm
2	0.5	Downward	160 rpm
3	2	Upward	150 rpm
4	6	Upward	150 rpm
5	2	Downward	235 rpm
6	6	Downward	235 rpm

airflow with experimental data from the literature [15]. In order to avoid the encumbrance due to heat sources and ambient ventilation, both UV and visible lamps were turned off and a low air exchange rate of 0.5 ACH was applied. Simulations for the remaining four cases were used to validate the model in terms of the average vertical speed at the horizontal section at a height of 2.44 m. For these four cases, the room was maintained at a slightly negative pressure of 12 Pa, and without UV irradiation or a microorganism source, as in a previously published experiment [10,11]. Simulations for Cases 5 and 6 were also performed to predict the fraction of microorganism remaining at the exhaust (see Section A in Fig. 1) for comparison with the experimental results reported in the literature [10,11].

2.3. Grid system

The simulation domain of the chamber was made up of 65,803 surface meshes and 1,503,413 spatial cells generated by the Polyhedral Mesher of the commercial CFD software Star-CCM+ V6.04.014 [17]. As a whole, a good grid quality was ensured with the maximum skewness angle to be less than 81° [18]. In order to appropriately simulate the air movement induced by the rotation of the fan blades, over 86% of spatial cells were located in the rotational region, which was only 6.7% of the simulation field. In addition, the prism cell layers were applied on all of the wall boundaries, and those along the fan blades were made very thin to ensure sufficient grid resolution in order to capture the flow characteristics in the near-wall region of the blades (Fig. 2).

2.4. CFD methods

With Star-CCM+ V6.04.014 [18], the realizable $k-\epsilon$ model [19] which was considered more reliable than the standard $k-\epsilon$ model for simulating rotational shear flow, was combined with a two-layer approach [20] using the Wolfstein model [21]. This combination was adopted together with the implicit SIMPLE algorithm [22]. The finite volume method was applied with the second-order upwind scheme for discretizing the governing equations of velocity components and pressure, and the first-order upwind scheme for temperature and passive scalar. For the near-wall region, the all- y^+ wall treatment was applied to emulate the high y^+ wall treatment with standard wall laws for $y^+ > 30$, the low y^+ wall treatment for fine meshes with y^+ to be approximately 1 or less to give reasonable results for intermediate meshes where the cell centroid fell in the buffer layer.

The rotating reference frame was applied only in the rotational region by assuming that the region was in a quasi-steady state. This method did not explicitly model rotation; instead, it generated a constant grid flux in the appropriate conservation equations by automatically adding the source terms with respect to the Coriolis force and Centrifugal force, which were calculated with Equation (1) based on the properties of the reference frame. Although this method underestimates the weak effect, it is appropriate for the flow, which is most likely to be influenced by time-averaged

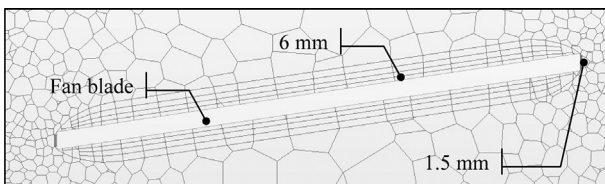


Fig. 2. Prism cell layers around the fan blades.

properties. A significant amount of simulation time can be saved with this method, when compared to simulating the ceiling fan's rotation in a transient state [18].

$$F_r = \rho\omega \times v \quad (1)$$

where, F_r was the body force term due to fan rotation [$\text{kg}/\text{m}^2 \text{ s}^2$], ρ was the air density [kg/m^3], ω was the rotational speed [rad/s], and v was the linear velocity [m/s].

2.5. Boundary conditions

The boundary conditions are listed in Table 2. In Cases 3, 4, 5 and 6, to include the heat effect of the UV and visible lamps in the simulation, it was assumed that 75% of the electrical input was transformed into heat loss [23], among which 40% was by convection, 40% by infrared radiation and 20% by conduction [24]. When the lamps were turned on, heat loss due to convection was set at the lamp surfaces, and that due to infrared radiation and conduction from the UV and visible lamps was assumed as convective heat transfer from the wall. In the simulations with the lamps turned on, a uniform heat transfer rate was set at the wall surfaces with the total amount equal to the heat loss due to infrared radiation and conduction from the UV and visible lamps. In addition, in these four cases, the boundary conditions for the ball source were determined from the experimental settings of First et al. [10]. In their experimental facility, the microorganisms aerosolized by a 6-jet Collison nebulizer (CN 25, BGI Inc., USA) entered the center of the room through a tube with a perforated ball at its end, which distributed the aerosols evenly in all directions.

2.6. Calculation of fraction of microorganism remaining by Eulerian method

A previous numerical study performed on the same chamber environment indicated that much more computational cost and more post processing efforts were required for the particle tracking with the Lagrangian method compared to the passive scalar simulation with the Eulerian method [14]. Because this study aimed to provide an efficient numerical tool for assessing the UR-UVGI disinfection efficacy, the Eulerian method was preferred. This method calculated the dispersion process of airborne particles by representing it with a passive scalar movement together with indoor air. According to the experimental procedures by First et al.

Table 2
Boundary conditions.

Item	Boundary conditions
Inlet	Size: 0.34 m × 0.34 m; velocity: 0.05 m/s in Cases 1 & 2, 0.2 m/s in Cases 3 & 5 and 0.6 m/s in Cases 4 & 6; temperature: 21.1 °C; turbulence intensity: 0.05; turbulence length scale: 0.0016 m
Outlet	Size: 0.48 m × 0.28 m; free slip
UVGI fixture	No slip; convective heat transfer rate: 48.3 W/m² (10 W per unit)
Visible lamp	No slip; convective heat transfer rate: 50.7 W/m² (total 57 W)
Source	In simulations without source (Cases 1 & 2): adiabatic wall, no-slip; in simulations with source (Cases 3, 4, 5 & 6): inlet, velocity: 0.012 m/s (12 L/min); temperature: 21.1 °C; turbulence intensity: 0.05; turbulence length scale: 0.00003 m
Ceiling fan	No slip, adiabatic
Walls	No slip, convection heat transfer rate: 1.18 W/m² when UVGI was turned off, and 2.01 W/m² when UVGI was turned on

[10], microorganisms were added to the chamber by attaching on the surfaces of the aerosols with a diameter of less than 2.5 μm , which were generated continuously at a constant rate and sampling was performed after steady state was closely achieved. Therefore, it should be appropriate to simulate the microorganism concentration using a passive scalar at a steady state. The UV inactivation of airborne microorganisms was coupled in the transport equation as follows:

$$\frac{\partial \phi}{\partial t} + \frac{\partial}{\partial x_j} (\phi u_j) = \frac{\partial}{\partial x_j} \left((\lambda + \lambda_t) \frac{\partial \phi}{\partial x_j} \right) - Z E_P \phi \quad (2)$$

Here, ϕ was the concentration of the microorganism [cfu/m^3], u_j were the velocity components [m/s], λ was the molecular diffusivity [m^2/s], λ_t was the kinematic diffusivity [m^2/s], Z was the UV susceptibility constant of the microorganism [m^2/J], and E_P was the UV fluence rate at a point P [W/m^2].

Bacillus atrophaeus spores were used in the experiments [10,11] with the UV susceptibility constant to be 0.04 m^2/J . In the simulations, the *B. atrophaeus* spores were represented as a passive scalar with a Schmidt number of 1. Because the fraction of microorganism remaining was calculated as the non-dimensional ratio of the concentration of *B. atrophaeus* spores measured with the UVGI turned on to the concentration measured with the UVGI turned off, the concentration at the microorganism source was arbitrarily set to be 1 cfu/m^3 .

The death rate of microorganisms in the air was influenced by several factors, such as air temperature, relative humidity, and disinfection by UV irradiation. When considering airborne transmission by droplet nuclei and ignoring the evaporation process of droplets, the death rate caused by the factors other than UV irradiation could be simplified to be a constant value [25]. This value was much lower than the death rate caused by UV irradiation in a room with perfect mixing ventilation. The ignorance of this value in concentration simulation could take fewer effects on the prediction of the fraction of microorganism remaining, e.g. the ratio of the concentration of airborne microorganisms with UVGI turned on to the one with UVGI turned off, which was of primary interest in this study. Therefore, as well as in the experiments [10,11], we assumed in the simulation that the inactivation of the microorganisms was only caused by UV irradiation.

The spatial distribution of UV fluence rates within the irradiation zone was obtained from a commercially available Computer-Aided Design (CAD) tool named Visual™ (Acuity Brand Lighting, Conyers, GA). The CAD tool is widely used by the lighting industry for analysis of architectural lighting layouts, and its application has been extended to the prediction of UV fluence rate, based on the same algorithms to perform calculations in the visible range of the spectrum. Details of the CAD procedure can be found in the paper by Rudnick et al. [26]. When applying Visual™ to calculate the UV fluence rate in UV irradiation zone, the reflectivity was assumed to be 10% [26]. In addition, an interpolation function by Star-CCM+ V6.04.014 was applied to map the UV fluence rate distribution by Visual™ onto the CFD grid.

3. Results

We first examined the fluence rate distribution generated by the CAD tool and the interpolation process of the CFD tool; next we investigated the fan-induced airflow reproduced by CFD simulations in an environment with very little ventilation; finally we investigated the capability of the CFD method to predict the vertical air speed and UR-UVGI disinfection efficacy in terms of the fraction of microorganism remaining when using a ceiling fan.

3.1. Fluence rate distribution

Relative agreement between the physical measurement with a cylindrical sensor and the numerical prediction by the CAD tool was quantified graphically with the Bland–Altman plot in terms of the fluence rates at 72 specific locations within the UV irradiance zone as shown in Fig. 3. The Bland–Altman plot [27] is a graphical approach for evaluating agreement between a pair of numbers obtained by two different methods. The details can be found elsewhere [26].

According to Fig. 3, approximately 97% of the ratios of measured to predicted fluence rates fell between the upper and lower 95% limits of agreement (LOA), which corresponded to the mean difference between the pairs of ± 1.96 standard deviations of the differences. However, because the UV lamp output was collimated by the louvers, the irradiance field from the UV fixture contained discontinuities, which could change very abruptly and cause poor prediction at a particular location close to the fixtures. Fig. 4 shows the symmetrical distribution of fluence rates at the horizontal section 2.2 m above the floor, which was obtained after the interpolation process by Star-CCM+ [18]. The average UV fluence rate of the irradiation zone was 0.15 W/m^2 .

3.2. Fan-induced airflow

Momoi et al. [15] measured the detailed air velocity distribution around a ceiling fan in a large experimental room where the ambient ventilation was believed to be very small and unable to affect fan-induced airflow. The comparison of experimental and CFD results is presented in Figs. 5 and 6 for Cases 1 and 2, respectively. As shown in Table 3, the CFD model was different from the experimental settings in terms of the room size and ceiling fan. However, because the conditions of the ambient environment and fan operation in the simulation were similar to those in the experiment, it was reasonable to qualitatively investigate the CFD method's capability of correctly reproducing the fan-induced

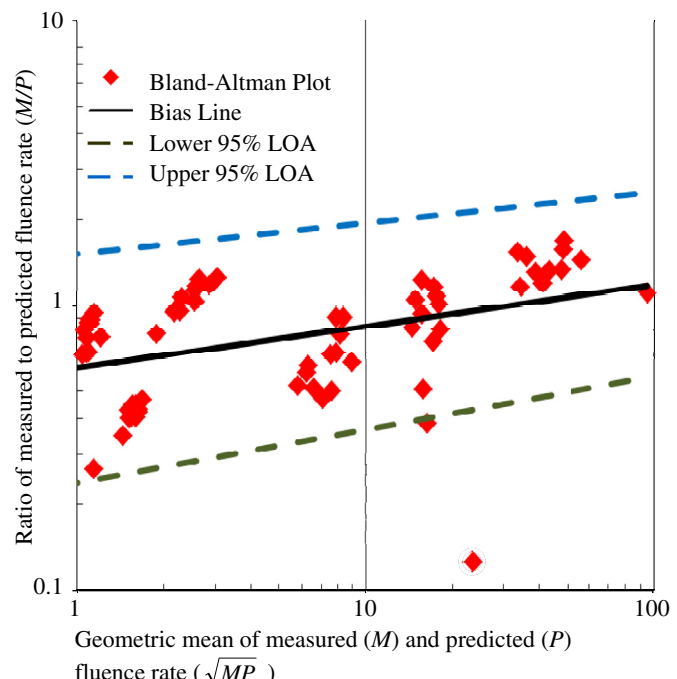


Fig. 3. Comparison of measured and predicted UV fluence rate.

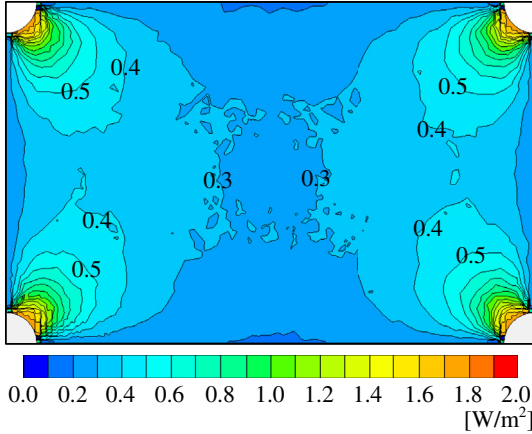


Fig. 4. UV fluence rate distribution in the horizontal section 2.2 m above the floor.

airflow by comparing the spatial variation trends of the velocity components.

According to Figs. 5 and 6, the CFD simulations reproduced the fan-induced airflow well, and characterized the flow field around the ceiling fan regardless of the fan rotational direction. Additionally, the simulation results were also consistent with the experimental data in terms of the change of velocity components in the direction along the fan blade at the height of 20 cm above and below the fan blade. 85% of the differences between the velocity components due to simulation and measurement were smaller than 0.25 m/s. The greatest difference was for the vertical velocity component in Case 2 (V_z in Fig. 6(c)). As a whole, considering the differences between the experimental and CFD settings, we judged that the simulated values of the velocity components were reasonable and acceptable. Therefore, this CFD modeling method with a rotating reference frame indicated sufficient accuracy to reproduce the flow field around an operating ceiling fan regardless of its rotational direction and speed.

In addition, the floor and walls showed great influence on fan-induced airflow. In such a small confined space, the use of a ceiling fan generated large-sized air circulations between the central

line of the room and sidewalls. Furthermore, the downward fan-induced airflow generated additional small-sized air circulation between the floor and the fan-induced airflow. These fan-induced air circulations could contribute to the mixing of room air. However, the downward fan-induced airflow also generated eddies between the fan-induced airflow and sidewalls in the lower portion of the room. This indicated the possibility of high local concentration of the microorganisms and elevated infection risk in case that there was no efficient infection control measure, such as UR-UVGI.

3.3. Average vertical air speeds

The average vertical air speeds due to the experiment and simulation were compared in Table 4 for Cases 3, 4, 5 and 6. In the experiment, the horizontal section 2.44 m above the floor was divided into 16 equal-area rectangles, and the velocity was measured 100 times at an interval of one second at the center of each of these rectangles. In each case, the average vertical air speed was the average of the absolute values of these 1600 measurements without regard for the airflow's direction [11]. Furthermore, the simulation result in each case was calculated as the average of the absolute values of the vertical air velocities at the centers of the rectangles. According to Table 4, the average vertical air speeds were predicted with errors of less than 10%, and the prediction accuracy was better when the air exchange rate was 6 ACH.

As shown in Fig. 7, fan-induced airflow dominated the air movement indoors even when the air exchange rate was as high as 6 ACH regardless of the fan rotational direction and speed. For example, in the horizontal Section C (see Fig. 1), which was 0.95 m under the fan blades and at the height of the breathing zone of a person while standing, the flow field was characterized by the ceiling fan's rotational conditions. On the other hand, in such a small chamber, the walls indicated an important factor in forming the indoor airflow pattern when using the ceiling fan.

The CFD method correctly reproduced the fan-induced airflow and reflected its impact on the indoor flow field. However, in the horizontal section, which was only 4 cm below the fan blades, the velocities were very sensitive to the location and time due to the influence by the walls and the rotation of the fan blades. It was a difficult task to accurately predict the temporary local velocities in

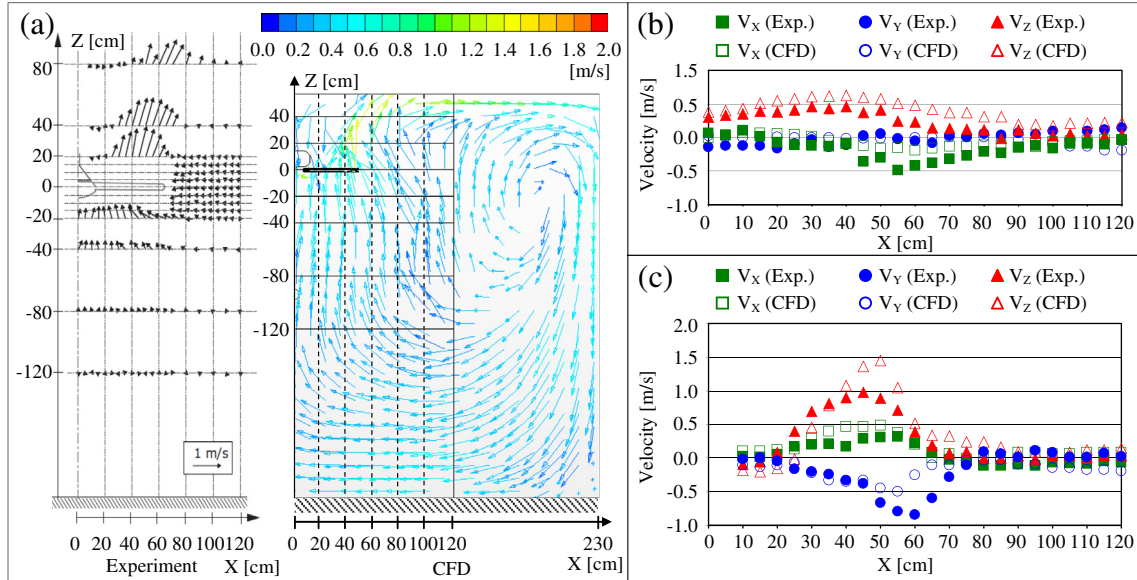


Fig. 5. Comparison of fan-induced airflow due to experiment and CFD in Case 1 (0.5 ACH & upward 160 rpm): (a) comparison of velocity distribution around ceiling fan; (b) comparison of velocity components 20 cm above the fan blades; (c) comparison of velocity components 20 cm below the fan blades.

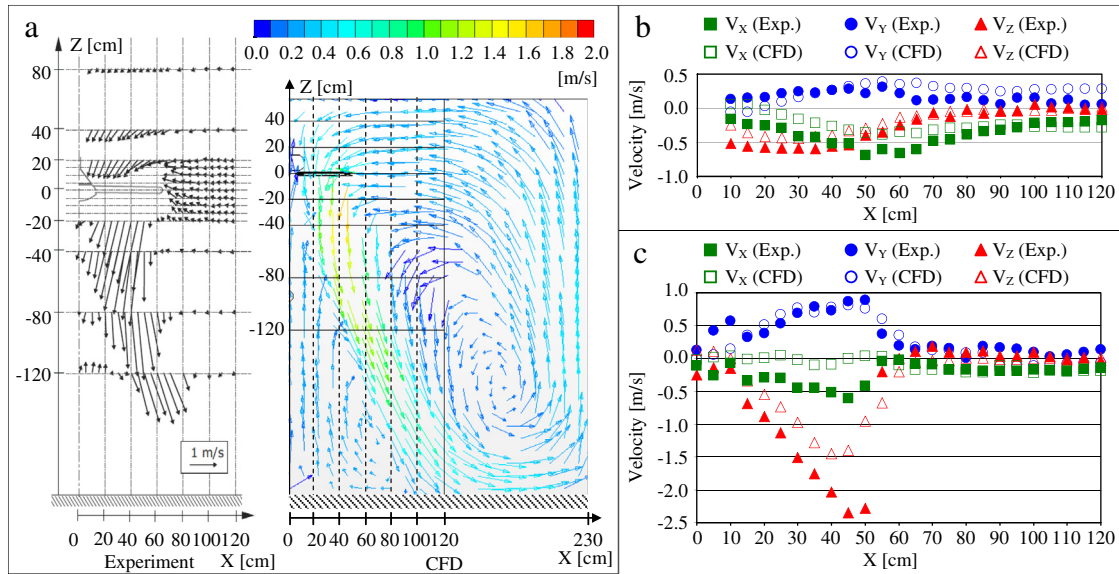


Fig. 6. Comparison of fan-induced airflow due to experiment and CFD in Case 2 (0.5 ACH & downward 160 rpm): (a) comparison of velocity distribution around ceiling fan; (b) comparison of velocity components 20 cm above the fan blades; (c) comparison of velocity components 20 cm below the fan blades.

Table 3
Differences between simulations and experiments in Cases 1 and 2.

Parameter	In simulations	In experiments of Momoi et al. (2004)
Chamber size	(L)4.6 m × (W)2.97 m × (H)3.05 m	A large chamber with both length and width over 3 m, 4.25 m at height
Fan	Maker: Hunter Fan Company, Model: MOD-CAT 20466-300. Have 5 blades with the length of 0.46 m (0.56 m from center of fan housing to blade tip). Fan blades located 2.48 m above the floor	Maker: Matsushita Electric Industrial; Model: F-M131 H-W. Have 3 blades with the length of 0.53 m (0.65 m from center of the motor housing to blade tip). Fan blades located 2 m above the floor.

this section with the simplified simulation in a steady state. However, as such good agreement on the average vertical air speed was obtained even in this horizontal section so close to the fan blades, this numerical method could be considered appropriate to predict the air mixing effect of a ceiling fan, which was one of the most important purposes to develop this CFD method.

3.4. Fraction of microorganism remaining based on Eulerian method

Figs. 8 and 9 shows the microorganism concentration distributions in Section B and C (see Fig. 1) in Cases 5 and 6 with a downward rotational speed of 235 rpm. The concentration was lower close to the inlet. In addition, in each case, the microorganism concentration with UR-UVGI turned on decreased by over 33% in most of the room space, compared to the concentration obtained when the UR-UVGI turned off. It coincided with the results presented in Table 5, which compared the volume-averaged concentration in Cases 5 and 6 with UR-UVGI turned on and off, respectively. According to Figs. 8 and 9, and Table 5, UR-UVGI disinfection efficacy was greater when applying a smaller air

exchange rate as the concentration decrease caused by the application of UR-UVGI was greater in Case 5. On the other hand, a higher air exchange rate helped to more efficiently decrease the concentration by more quickly exhausting the microorganisms to the outside, which resulted in the concentration distribution to be smallest in Case 6 with UR-UVGI turned on.

The fractions of microorganism remaining obtained from experiments and simulations were compared in Table 6. In the experiment by First et al. [11], *B. atrophaeus* spores were sampled directly in front of the midpoint of the exhaust air grille in Cases 5 and 6 with high downward fan rotational speed. Therefore, we calculated the fraction of microorganism remaining based on CFD results with the concentrations at the midpoint of the exhaust (see Section A in Fig. 1). In addition, this parameter was also calculated with the volume-averaged concentrations, in order to examine the fraction of microorganism remaining in the whole room.

As the air in the chamber was well mixed in these two cases, the simulation results with the concentration at the midpoint of the exhaust and the volume-averaged concentration were consistent with each other. The prediction of the fraction of microorganism remaining was accurate in Case 5 with the air exchange rate of 2 ACH. However, the fraction of microorganism remaining by CFD was poor and there was an evidently underestimated value in Case 6 with the air exchange rate of 6 ACH.

According to Table 6, as well as the experimental result, the simulated fraction of microorganism remaining also increased with the air exchange rate when the fan blew air downward at the same speed. Therefore, although this CFD modeling method failed to match the fraction of microorganism remaining in Case 6, it should

Table 4
Comparison of average vertical speed at the height of 2.44 m.

Case	Experiment [m/s]	CFD [m/s]	Error [%]
3	0.144	0.158	9.7
4	0.138	0.131	5.1
5	0.143	0.157	9.8
6	0.183	0.187	2.2

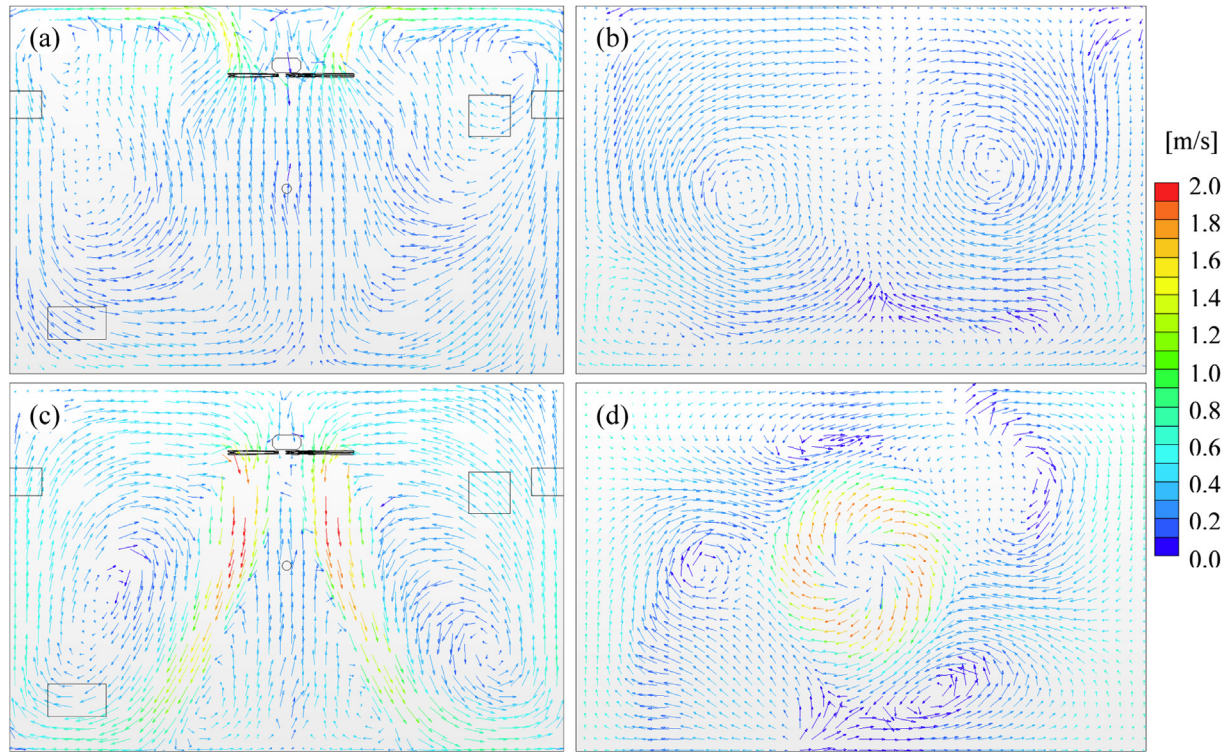


Fig. 7. Vector velocity distributions in Case 4 (6 ACH & upward 150 rpm) and Case 6 (6 ACH & downward 235 rpm): (a) in Section B in Case 4; (b) in Section C in Case 4; (c) in Section B in Case 6; (d) in Section C in Case 6.

be capable of investigating the UR-UVGI's disinfection performance when using a ceiling fan.

4. Discussion

Large differences were generated between the experimental and simulated results in terms of the fraction of microorganism remaining in Case 6. It resulted primarily from the limitations of CFD methods, room modeling, experimental errors, and differences between experimental and simulation conditions.

This study applied two simplified approaches in the numerical modeling to achieve significant reduction of expensive computations, at the cost of simulation accuracy. First, we used a rotating reference frame, which did not show the transient effect due to the real motion. Therefore, the simulated flow field and microorganism concentration distribution in the vicinity of the fan blades would be somewhat different from those in the real world. Unfortunately, the fan blades were inside the UV irradiation zone. This condition reduced the prediction accuracy of the UV exposure for microorganisms due to the ignorance of the transient effect. Second, we applied the Eulerian method by using a passive scalar to represent airborne particles, which derived microorganism concentration based on simultaneous effects of UV irradiation on the microorganisms. As shown in Equation (2), the UV susceptibility constant, which should vary for each particle with the microorganisms, was fixed at $0.04 \text{ m}^2/\text{J}$ in the simulation. The Eulerian method could not track the disinfection process for each infectious particle and consider the own survival rate for airborne microorganisms attached on the particle. Therefore, the inactivation mechanism due to Eulerian method was different from that in the real world, in which the inactivation probability of an infected particle was not linear to UV dose. Therefore, the Eulerian method would generate errors in predicting the UR-UVGI's disinfection effect.

There was a tradeoff between the accuracy of generating fan-induced airflow and the computational cost when determining the extent of the rotational region. According to the results of trial simulations, air movement in the vertical direction became violent and likely incorrect when the rotational region was much smaller; however, as the rotational region occupied over 86% of spatial cells, its expansion could result in a significant increase of spatial cells. Therefore, the practical motivation of avoiding too heavy a computational burden required the smaller choice of rotational region. Here, the border of the rotational region was initially proposed by the experienced supporter of the CFD tool, and finally determined after a number of trials, in consideration of the server's computational capability.

On the other hand, the experimental errors were also evidently great. In the biological experiment conducted in a real-size chamber, the fraction of microorganism remaining was measured to be over 1.0 in Case 6, which was physically impossible and an overestimate.

Finally, as a numerical tool, CFD worked well under the ideal conditions where there were not any interruptions to the flow and concentration fields. Therefore, the air mixing by a ceiling fan might be overestimated and there may have been a greater number of microorganisms to be inactivated by UR-UVGI in CFD. Moreover, due to the vibration caused by the motor's operation, the fan blades usually move in a much more complicated pattern in reality. However, in CFD simulation, the movement of fan blades was simplified as the rotation at a constant speed around a fixed axis. This simplification would affect the accuracy for CFD simulations to reproduce the fan-induced airflow.

5. Conclusions

In this study, a CFD modeling method was developed to assess the indoor air mixing and UR-UVGI disinfection efficacy when using a

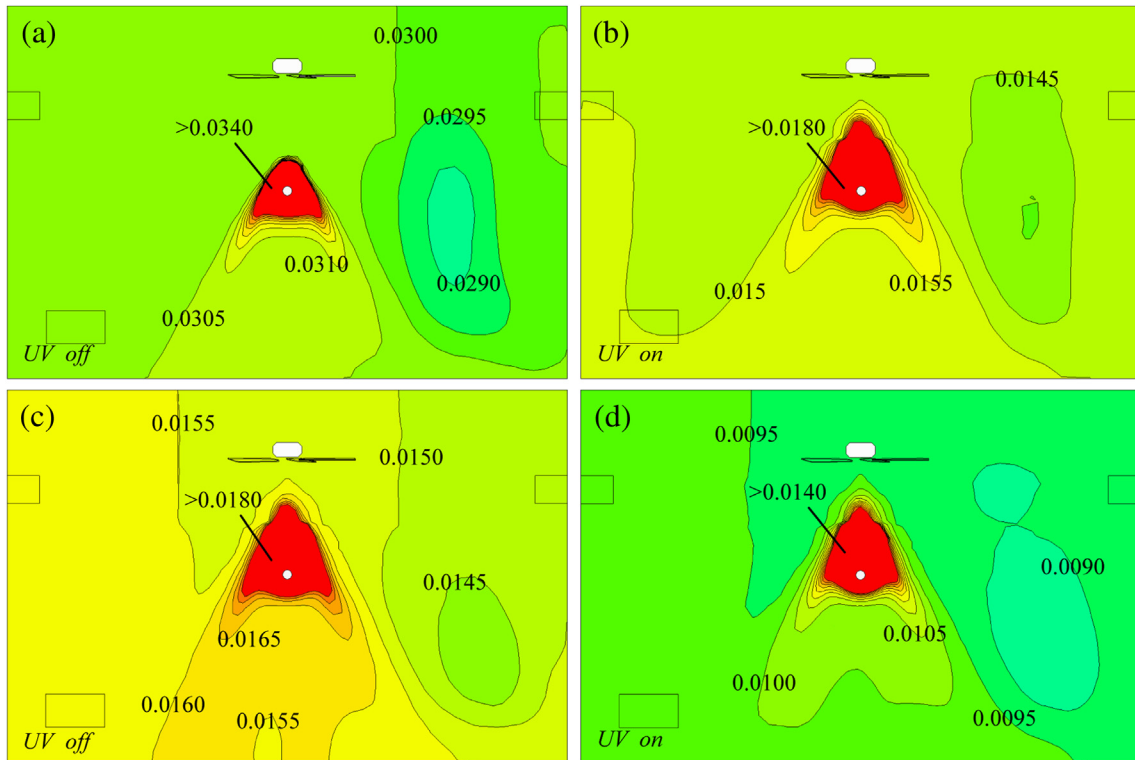


Fig. 8. Concentration distribution of microorganisms in Section B in Case 5 (2 ACH & downward 235 rpm) and Case 6 (6 ACH & downward 235 rpm) [cfu/m^3]: (a) in Case 5 with UV off; (b) in Case 5 with UV on; (c) in Case 6 with UV off; (d) in Case 6 with UV on.

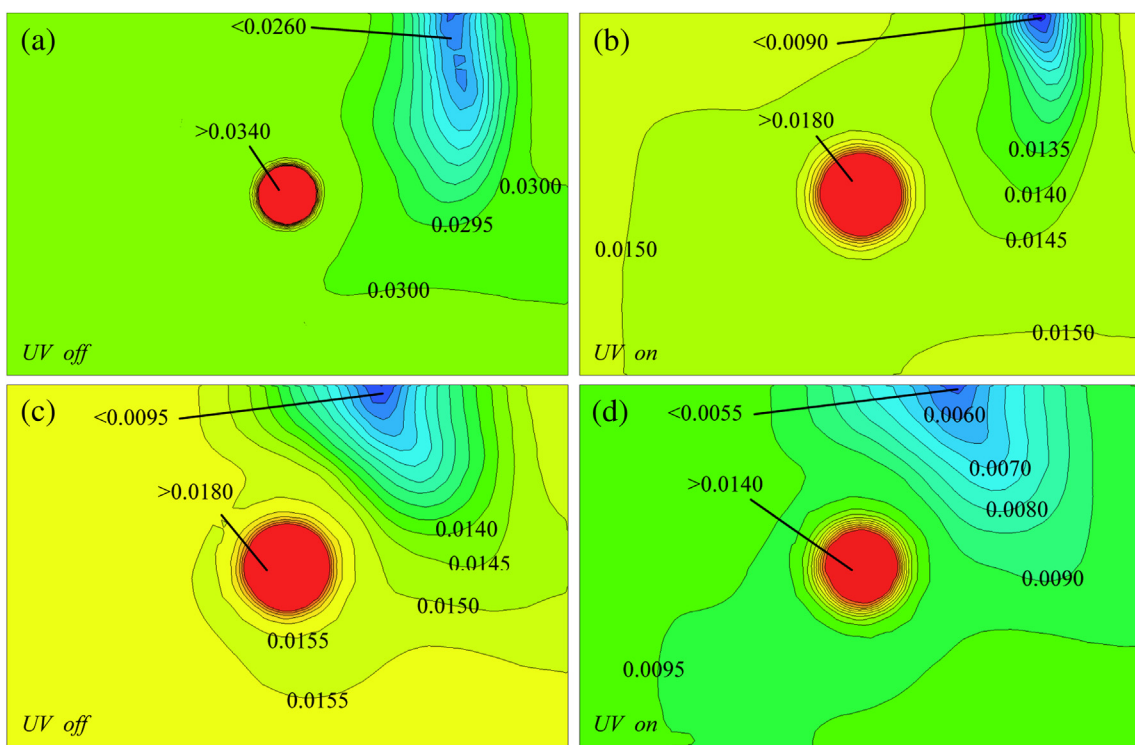


Fig. 9. Concentration distribution of microorganisms in Section C in Case 5 (2 ACH & downward 235 rpm) and Case 6 (6 ACH & downward 235 rpm) [cfu/m^3]: (a) in Case 5 with UV off; (b) in Case 5 with UV on; (c) in Case 6 with UV off; (d) in Case 6 with UV on.

Table 5

Simulation results of volume average of microorganism concentration in Cases 5 and 6 with different air exchange rate.

Case	Air exchange rate [ACH]	UR-UVGI off [cfu/m ³]	UR-UVGI on [cfu/m ³]	Concentration reduction due to the use of UR-UVGI [%]
5	2	0.0301	0.0149	50.5
6	6	0.0154	0.0095	38.3

Table 6

Comparison of fraction of microorganism remaining in Cases 5 and 6 with different air exchange rate.

Case	Experiment [%]	CFD (calculated with the concentration at exhaust) [%]	CFD (calculated with the volume average concentration) [%]
5	0.44 ± 0.13	0.50	0.50
6	0.88 ± 0.16	0.62	0.62

ceiling fan. With this method, the periodic fan rotation was simulated at a steady state by applying the rotating reference frame to reproduce the fan-induced airflow. Furthermore, the dispersion of airborne microorganisms was calculated with the Eulerian method by using a passive scalar to represent the airborne particles.

This CFD modeling method was validated by comparing its predictions to experimental data in terms of velocity and the fraction of microorganism remaining. The comparison showed that this method properly reproduced and characterized the fan-induced airflow, and the vertical air mixing by the ceiling fan. In addition, this method correctly predicted the fraction of microorganism remaining in Case 5. Furthermore, both CFD and the experiments predicted that the fraction of microorganism remaining in the chamber increased with the ambient air exchange rate when the fan blew air downward with a fan rotational speed of 235 rpm. Therefore, this method is able to predict the UR-UVGI disinfection efficacy when using a ceiling fan to improve indoor air mixing.

In the future, this CFD modeling method will be applied to conduct parametrical investigation of the integrated application of ceiling fan and UR-UVGI to improve the UR-UVGI's performance on inactivating microorganisms, with consideration of the various indoor settings with specified humidity, temperature, ambient ventilation, microorganisms, heat sources, and well characterized UV fixtures.

Acknowledgment

This study was supported by the Fogarty Grant project "Sustainable Air Design Technology Innovations for Resource Limited Settings" (Grant number: R24TW008821), which was funded under the American Recovery and Reinvestment Act (ARRA) of 2009 by Fogarty International Center, National Institutes of Health, USA. The authors would like to thank Dr. Melvin First in Harvard School of Public Health, who was the main member of the project and passed away in 2011, for his great contribution to the project.

References

- [1] WHO. WHO report 2012: global tuberculosis control. World Health Organization; 2011. Available: http://apps.who.int/iris/bitstream/10665/75938/1/9789241564502_eng.pdf [accessed 11.10.12].

- [2] Frieden TR, Sherman LF, Maw KL, Fujiwara PI, Crawford JT, Nivin B, et al. A multi-institutional outbreak of highly drug-resistant tuberculosis: epidemiology and clinical outcomes. *J Am Med Assoc* 1996;276(15):1229–35.
- [3] Breathnach AS, de Ruiter A, Holdsworth GM, Bateman NT, O'Sullivan DG, Rees PJ, et al. An outbreak of multi-drug-resistant tuberculosis in a London teaching hospital. *J Hosp Infect* 1998;39(2):111–7.
- [4] US-NIOSH. Environmental control for tuberculosis: basic upper-room ultraviolet germicidal irradiation guidelines for healthcare settings. Atlanta GA: United States National Institute for Occupational Safety and Health; 2009.
- [5] Ecombe AR, Moore DAJ, Gilman RH, Navincopa M, Ticona E, Mitchell B, et al. Upper-room ultraviolet light and negative air ionization to prevent tuberculosis transmission. *PLoS Med* 2009;6(3):e121–23.
- [6] Wells WF, Wells MW, Wilder TS. The environmental control of epidemic contagion I – an epidemiologic study of radiant disinfection of air in day schools. *Am J Epidemiol* 1942;35(1):97–121.
- [7] Riley RL, Permutt S. Room air disinfection by ultraviolet irradiation of upper air. Air mixing and germicidal effectiveness. *Arch Environ Health* 1971;22(2):208–19.
- [8] Riley RL, Permutt S, Kaufman JE. Room air disinfection by ultraviolet irradiation of upper air. Further analysis of convective air exchange. *Arch Environ Health* 1971;23(1):35–9.
- [9] Riley RL, Kaufman JE. Effect of relative humidity on the inactivation of airborne *Serratia marcescens* by ultraviolet radiation. *Appl Microbiol* 1942;23(6):1113–20.
- [10] First MW, Rudnick SN, Banahan KF, Vincent RL, Brickner PW. Fundamental factors affecting upper-room ultraviolet germicidal irradiation-part I. Experimental. *J Occup Environ Hyg* 2007;4(5):321–31.
- [11] Rudnick SN, First MW. Fundamental factors affecting upper-room ultraviolet germicidal irradiation-part II. Predicting effectiveness. *J Occup Environ Hyg* 2007;4(5):352–62.
- [12] Noakes CJ, Sleigh PA, Fletcher LA, Beggs CB. Use of CFD modelling to optimise the design of upper-room UVGI disinfection systems for ventilated rooms. *Indoor Built Environ* 2006;15(4):347–56.
- [13] Sung M, Kato S. Method to evaluate UV dose of upper-room UVGI system using the concept of ventilation efficiency. *Build Environ* 2010;45(7):1626–31.
- [14] Heidarinejad M, Srebric J. Computational fluid dynamics modeling of UR-UVGI lamp effectiveness to promote disinfection of airborne microorganisms. *World Rev Sci Technol Sustain Dev* 2013;10(1/2/3):78–95.
- [15] Momoi Y, Sagara K, Yamanaka T, Kotani H. Modeling of ceiling fan based on velocity measurement for CFD simulation of airflow in large room. In: Proceedings of 9th international conference on air distribution in rooms, Coimbra, Portugal 2004. pp. 145–50.
- [16] Momoi Y, Sagara K, Yamanaka T, Kotani H. Modeling of prescribed velocity generated by ceiling fan based on velocity measurement for CFD simulation. In: Proceedings of 10th international conference on air distribution in rooms, Helsinki, Finland 2007. pp. 1141–50.
- [17] Zhu S, Srebric J, Rudnick SN, Vincent RL, Nardell EA. Numerical investigation of upper-room UVGI disinfection efficacy in an environment chamber with a ceiling fan. *Photochem Photobiol* 2013;89:782–91.
- [18] CD-adapco. User guide of STAR-CCM+ 6.04.014; 2011.
- [19] Shih T-H, Liou WW, Shabbir A, Yang Z, Zhu J. A new k-ε eddy viscosity model for high Reynolds number turbulent flows-model development and validation. *Comput Fluids* 1994;24(3):227–38.
- [20] Rodi W. Experience with two-layer models combining the k-ε model with a one-equation model near the wall. In: Proceedings of 29th aerospace sciences meeting, Reno, NV 1991. p. 13.
- [21] Wolfstein M. The velocity and temperature distribution in one-dimensional flow with turbulence augmentation and pressure gradient. *Int J Heat Mass Transf* 1969;12(3):301–18.
- [22] Patankar SV. Calculation of the flow field. In: Numerical heat transfer and fluid flow. New York: Taylor & Francis; 1980.
- [23] Cavet Lumi Smart™, intelligent lighting controller-technical explanation and perception guide. Canada: Cavet Technologies Inc; 2010.
- [24] Dieker H, Miesner C, Puttjer D, Bachl B. Manufacturing LEDs for lighting and displays: comparison of different LED packages. In: Proceedings of SPIE, Berlin, Germany, 6797; 2007. p. 67901.
- [25] Qian H, Li YG, Nielsen PV, Huang XH. Spatial distribution of infection risk of SARS transmission in a hospital ward. *Build Environ* 2009;44(8):1651–8.
- [26] Rudnick SN, First MW, Sears T, Vincent RL, Brickner PW, Ngai PY, et al. Spatial distribution of fluence rate from upper-room ultraviolet germicidal irradiation: experimental validation of a computer-aided design tool. *HVAC&R Res* 2012;18(4):774–94.
- [27] Bland JM, Altman DG. Measurement in medicine: the analysis of method comparison studies. *Statistician* 1983;32(3):307–17.